Available online at www.sciencedirect.com
ScienceDirect
Journal of Power Sources 174 (2007) 414–420
JOURNAL OF POWER SOURCES
www.elsevier.com/locate/jpowsour

Microstructural characterisation of battery materials using powder diffraction data: DIFFaX, FAULTS and SH-FullProf approaches

M. Casas-Cabanas [a], J. Rodríguez-Carvajal [b], J. Canales-Vázquez [a], Y. Laligant [c], P. Lacorre [c], M.R. Palacín [a,*]

[a] *Institut de Ciència de Materials de Barcelona (CSIC), Barcelona 08913, Spain*
[b] *Laboratoire Léon Brillouin (CEA-CNRS), Saclay, 91191 Gif-sur-Ivette Cedex, France*
[c] *Laboratoire des Oxydes et Fluorures, UMR CNRS 6010, Université du Maine, 72085 Le Mans Cedex, France*

Available online 3 July 2007

Abstract

The microstructure of Li_2PtO_3, isostructural with Li_2MnO_3, and β-$Ni(OH)_2$ is analyzed from powder diffraction data using two approaches. Firstly, the recently developed FAULTS program (a modification of the DIFFaX program to allow refinement of the diffraction pattern) is used to include different amounts and types of stacking faults in the microstructural description of the material. This approach treats size effects mostly isotropically and assigns most of the anisotropic peak broadening to stacking faults. On the other hand, the FullProf program is also used to perform Rietveld refinement with microstructural models that treat the effects of anisotropic size and hence considers that this is the main contribution to broadening. The simultaneous use of these two approaches allows choosing the most adequate model in each particular case in order to obtain an accurate description of the microstructure of the material.

Keywords: Microstructure; Battery materials; Powder diffraction; Rietveld; DIFFaX; FAULTS

1. Introduction

Polycrystalline materials invariably contain imperfections that can deeply influence their physical, mechanical and chemical properties, and battery materials are not an exception to this rule. The microstructural characterisation of these materials is of essential importance as it may have an important effect upon the electrochemical properties. Powder diffraction is now one of the most widely used techniques available to materials scientists for studying the structure and microstructure of crystalline solids. Microstructural features can strongly modify diffraction line profiles, leading to broadened and occasionally shifted or asymmetric diffraction lines. These features include finite crystallite size, extended defects such as stacking faults and the existence of microstrains that induce fluctuations in cell parameters. Unfortunately, correlation between the diffraction line profile and microstructural features is not direct and, moreover, superposition of different phenomena is common which turns the microstructural characterisation of solids into a complex task.

So far, a widely used tool to interpret the diffraction data of one-dimensionally disordered systems is the DIFFaX program, [1] which allows the simulation of powder X-ray and neutron diffraction patterns of defective materials. However, simulation leads only to qualitative results. To overcome this issue we have developed the new FAULTS program, [2] a code based on DIFFaX that allows not only simulation but also refinement of the experimental pattern, thus yielding much more accurate results. Another commonly used tool for the structural characterisation of matter is the Rietveld method, also based in diffraction patterns refinement, which can include specific microstructural models.

In this paper, we present two case examples of materials with different microstructural characteristics that have been studied by using both approaches: FAULTS and Rietveld refinement. For the latter we have used the FullProf program [3] that can model anisotropic size broadening with linear combinations of spherical harmonics (SH) [4]. While the FAULTS program assigns anisotropic line broadening to stacking faults and simulates size effects mainly isotropically, the SH approach reproduces anisotropic size broadening but cannot model the broadening caused by stacking faults. These assumptions have to be kept in mind when analyzing microstructural features.

* Corresponding author.
E-mail address: rosa.palacin@icmab.es (M.R. Palacín).

0378-7753/$ – see front matter © 2007 Published by Elsevier B.V.
doi:10.1016/j.jpowsour.2007.06.216

The first example is Li_2PtO_3 which has been studied as cathode material for lithium batteries and has been reported to have a volumetric capacity comparable to $LiCoO_2$ [4]. This compound is isostructural with Li_2MnO_3 and Li_2PdO_3 and it is also constituted of alternate Li and Li/Pt layers with oxygen in between. Similarly to Li_2MnO_3 [5], the XRD pattern of this material exhibits some reflections at low angles that are indicative of a honeycomb ordering of the lithium/transition metal layers and the Warren shape of the diffraction peaks certainly indicates the presence of stacking faults within the structure.

The second example is β-$Ni(OH)_2$, used as the positive electrode material in nickel batteries for more than a century, for which it is now generally accepted that lack of perfection in crystallization must be taken as a sine qua non reason for electroactivity. The X-ray diffraction patterns of the electroactive materials present anisotropic abnormal peak broadening that was commonly considered to be originated by to stacking faults [6]. In agreement with this, previous works in DIFFaX simulations [7,8] showed that certain amounts of stacking faults could result in anisotropic peak broadening.

2. Experimental

Li_2PtO_3 was prepared according to the method described in reference [4] and was always contaminated by small amounts of Pt. The X-ray powder diffraction pattern of this compound was recorded with a SiemensD-501 with Cu $K\alpha_1 = 1.5406$ Å, Cu $K\alpha_2 = 1.5444$ Å radiation in the range $2\theta = 14$–124° at a 0.02° scanning step. The instrumental resolution function (IRF) was obtained from a well crystallized La_2CrO_6 sample.

For the β-$Ni(OH)_2$ case, two samples with different microstructural characteristics were prepared. Sample S1 was obtained by addition of nickel nitrate 1 M to 28% NH_4OH at 60 °C in potassium hydroxide 5 M [9] and sample S2 was synthesized by direct precipitation of β-$Ni(OH)_2$ from a 1 M solution of nickel sulphate with 2 M sodium hydroxide at 70 °C [8]. This later method is widely used in the industrial preparation of electroactive β-$Ni(OH)_2$. Finally, an industrial commercial sample was also studied (sample I) that contains cobalt as a doping element. Its chemical composition was found to correspond to $Ni_{1-x}Co_x(OH)_2$ ($x = 0.012$). β-$Ni(OH)_2$ X-ray diffraction patterns were collected using a Siemens D-500 diffractometer with Cu $K\alpha_1 = 1.5406$ Å, Cu $K\alpha_2 = 1.5444$ Å radiation in the range $2\theta = 5$–105° at a 0.03° scanning step. The samples were side loaded in order to minimize texture effects and the IRF was obtained from a LaB_6 standard material.

The FAULTS program, as DIFFaX, needs an input file where the defective structure has to be described in terms of a stacking sequence of layers of atoms. Each type of layer can interconnect with the others via stacking operations that occur with a certain probability. In order to describe the defective layered structure, it is necessary to define the unit cell, the atomic positions in each layer type and the stacking/transition vectors. In the β-$Ni(OH)_2$ case, size effects were also taken into account as FAULTS allows the refinement of the size parameters that correspond to the Gaussian (D_g) and Lorentzian (D_i) contributions to the full width at half maximum (FWHM) [10]. In order to include a certain degree of size anisotropy, as β-$Ni(OH)_2$ samples exhibit a platelet-like morphology, the number of layers per crystallite was also considered. The quality of the agreement between observed and calculated profiles is given by the conventional R_p value [11].

Rietveld refinements were carried out with the FullProf program (Windows version, April 2004) using the pseudo-Voigt profile function of Thompson et al. [12]. To treat anisotropic size effects the Lorentzian part of the peak broadening was modeled with linear combinations of spherical harmonics (SH) which allow the calculation of the crystallite average size along each reciprocal lattice vector. An average apparent shape of the crystallites can also be displayed using the GFOURIER 04.02 program [13].

3. Results and discussion

3.1. Microstructural analysis of Li_2PtO_3

The powder X-ray diffraction pattern recorded is in full agreement with that described in reference [4]. Li_2PtO_3 is isostructural with Li_2MnO_3 [5] and Li_2PdO_3 [14], and can be indexed with the *C*2/*m* space group. The superstructure peaks in the range $2\theta = 17$–32° indicate that the Li/Pt atoms of the mixed layer are arranged following a "honeycomb" ordering scheme (see Fig. 1).

Rietveld refinement of Li_2PtO_3 using the FullProf program and the *C*2/*m* space group leads to refined cell parameters with values $a = 5.190(4)$ Å, $b = 8.983(2)$ Å and $c = 5.112(3)$ Å, and $\beta = 109.9(1)^\circ$. However, as it is shown in Fig. 2, Rietveld refinement is unable to model the Bragg intensities and the Warren fall that appears in the $2\theta = 20$–35° angular range (shown in the inset of Fig. 2), which indicates, as for Li_2MnO_3, a certain degree of short range disorder that may be due to defects in the stacking arrangement of the honeycomb layers. For the refinement of stacking faults the FAULTS program was used. Fig. 3 shows two

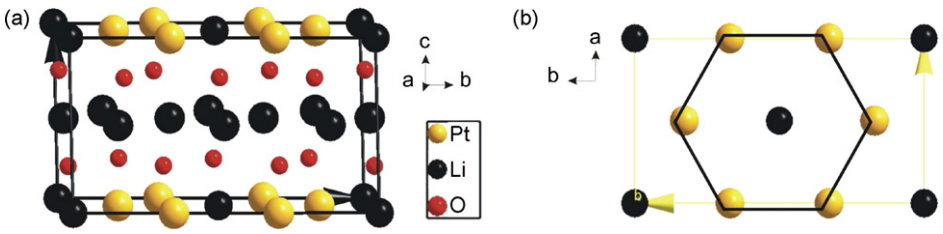

Fig. 1. (a) Li_2PtO_3 C2/m unit cell and (b) view of the Li/Pt layers where the honeycomb arrangement can be observed.

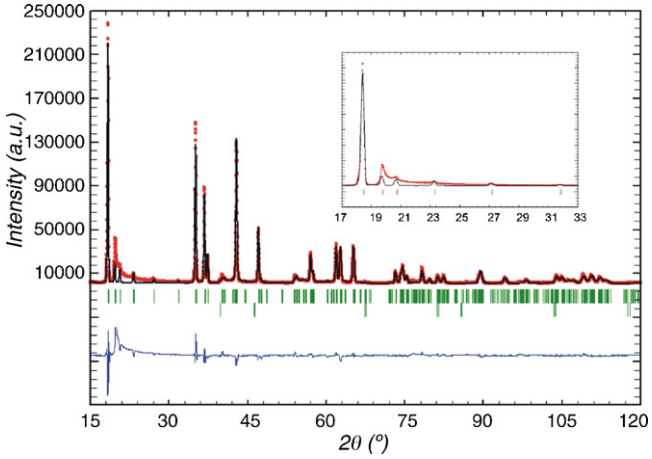

Fig. 2. Experimental X-ray powder diffraction pattern (dotted curve) compared to the Rietveld-refined profile (continuous line) and difference curve for Li_2PtO_3 by using the space group $C2/m$ ($R_p = 24.5$).

possible rotational displacements for the Li/Pt layers that would result in stacking faults. These can be described with two types of layer displacements as displacements 1, 3 and 5 are identical as well as displacements 2, 4 and 6.

In order to gain in computational speed, a smaller cell was chosen for the refinement with space group P-1 and $a = 5.1874$ Å, $b = 5.1874$ Å and $c = 5.1123$ Å, with angles $\alpha = 80.193°$, $\beta = 99.807$ and $\gamma = 60.039°$. In Fig. 4a, the two equivalent cells can be visualized. The FAULTS program imposes the stacking direction to be perpendicular to a and b axis and hence a new cell c parameter had to be calculated ($c' = 4.8069$Å) and an additional shift of (−1/6, 1/6, 0) had to be included in the layer stacking in order to describe the atomic positions corresponding to the new cell (see Fig. 4b).

The unit cell was divided into two structurally different layer types: the honeycomb composite block constituted of Li and Pt (layer 1) and another layer with the remaining atoms (layer 2). Two additional layers (layers 3 and 4), structurally identical to layer 1 were used to account for the rotational stacking faults shown in Fig. 3 through stacking vectors. Only transitions between layers 1–2, 3–2 and 4–2 were permitted. With this description, the ideal stacking (that was used in the Rietveld refinement) would consist of a stacking of types 1 and 2 layers alternatively and substitution of some type 1 layers for some types 3 and 4 layers would yield to the faulted structure. The refined stacking probabilities (α_{32} and α_{42}) would correspond directly to the amount of stacking faults.

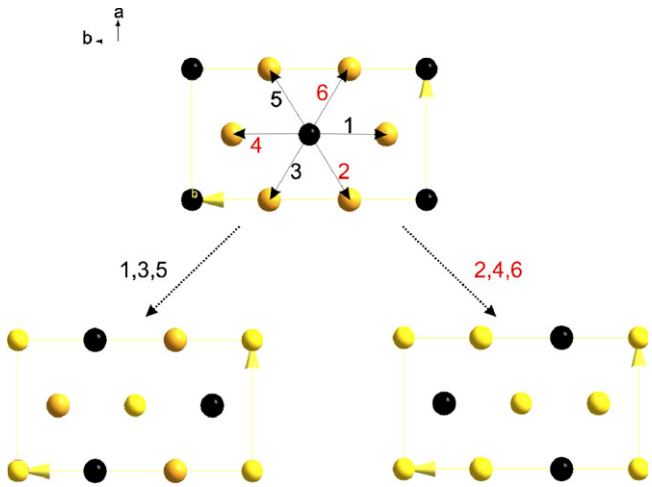

Fig. 3. Possible layer transitions that would lead to rotational stacking faults in the crystal structure of Li_2PtO_3. Translations 1, 3 and 5 are identical as well as transitions 2, 4 and 6.

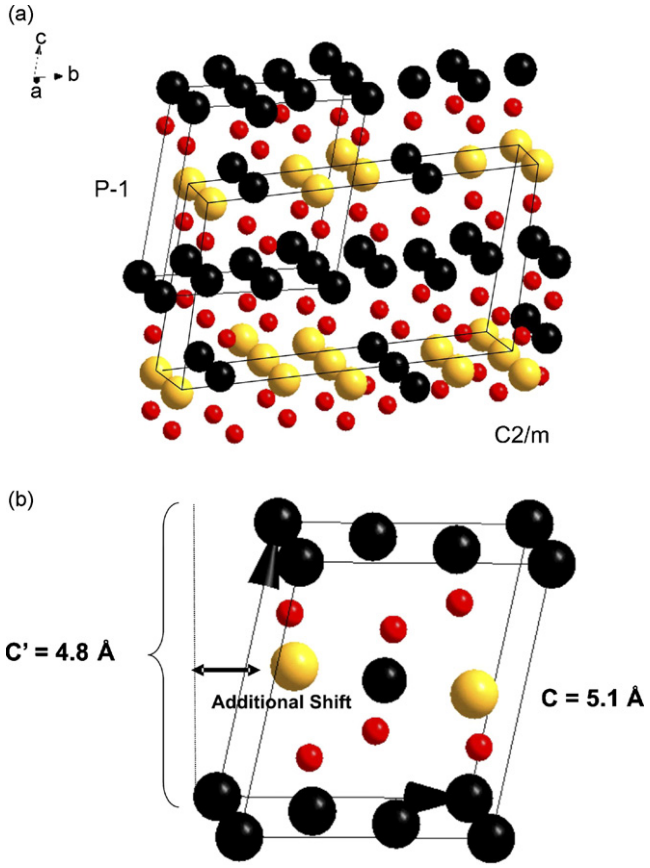

Fig. 4. (a) View of the Li_2PtO3 lattice where two cells can be visualized: monoclinic original cell with space group $C2/m$ and new smaller triclinic cell with space group P-1. (b) Conversion of this P-1 cell to the FAULTS adapted unit cell: c' axis, perpendicular to a and b, and additional stacking shift.

Fig. 5 depicts a comparison of the FAULTS-refined profile with the experimental one. No size broadening was necessary to model peak broadening and the background was modeled by linear interpolation. The best agreement ($R_p = 10.69$) was obtained for a sample with 39.5% of sequences 1–2, 30.4% of sequences 3–2 and 30.1% of sequences 4–2. Though no special ordering of the sequences was considered in the layer stacking description, an explicit sequence of layers was needed in order to avoid excessive broadening of the peaks at $2\theta = 20$–$25°$. This phenomenological treatment may be indicative some kind of ordering in the stacking sequence that is still under investigation.

3.2. Microstructural analysis of β-Ni(OH)$_2$

β-Ni(OH)$_2$ crystallizes in a brucite type structure (space group P-3m1) that can be described as an hexagonal close

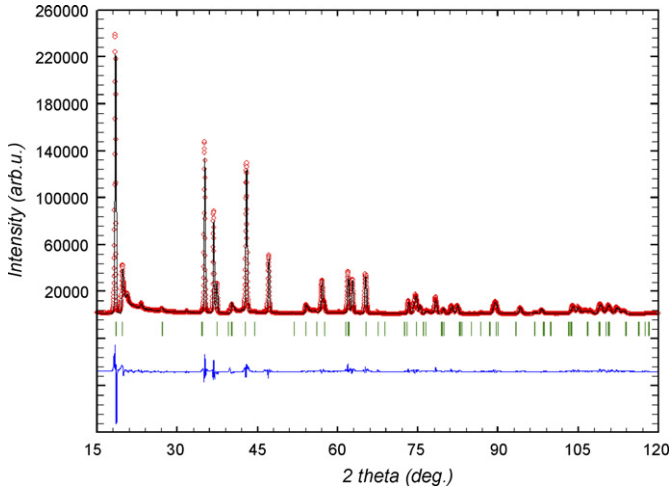

Fig. 5. Experimental X-ray powder diffraction pattern (dotted curve) compared to the FAULTS-refined profile (continuous line) and difference curve corresponding to sample Li_2PtO_3.

packed structure of hydroxyl ions, with AB oxygen packing, and Ni(II) occupying octahedral interstices one plane out of two, in C positions (see Fig. 6). The unit cell parameters are $a = 3.126$ Å and $c = 4.593$ Å [15]. The XRD pattern of electroactive β-Ni(OH)$_2$ suffers from a strong anisotropic diffraction peak broadening.

Stacking faults appear when one sheet of oxygen atoms shifts to position C, resulting in an ABC sequence. If the following sheet of oxygen atoms is located in the same position as two positions below, ABCB configuration, a growth type stacking fault is obtained. In contrast, if the following sheet of oxygen atoms is located in the same site as three positions below, ABCA configuration, the result is a deformation type stacking fault [16]. Considering both types of stacking faults, the oxygen sequence can be described with four types of layers [7], each one containing two sheets of oxygen atoms: AB (layer 1), CA (layer 2), BC (layer 3) and CB (layer 4). With this description, the ideal stacking would be represented by a sequence of type 1 layers with transition vector (0, 0, 1), which means that the displacement from layer 1 to layer 1 corresponds simply to the cell parameter c. The refined values for the stacking probabilities correspond directly to the amount of stacking faults in the structure: the extent of deformation faults can be obtained from the stacking

Table 1
Structural and microstructural FAULTS-refinement results for samples S1, S2 and I: stacking probabilities, size parameters and agreement factor R_p

Parameter	S1	S2	I
a (Å)	3.126	3.122	3.124
c (Å)	4.605	4.642	4.625
zO (Å)	0.2312	0.2252	0.2212
$D_g^{-1} \times 10^3$ (Å)	1.88	0.7	3.08
$D_l^{-1} \times 10^3$ (Å)	1.00	10.48	4.03
Number of layers	30	7	22
α_{11} (%)	96.4	52.29	88.1
α_{12} (%)	2.1	15.3	11.9
α_{14} (%)	1.5	31.8	0
R_p	7.47	6.77	8.27

probabilities between layers 1 and 2 (α_{12}), whereas the extent of growth faults corresponds to the stacking probability between layers 1 and 4 (α_{14}).

The refined parameters for the three samples studied are summarized in Table 1.

The number of stacking faults increases in the sequence S1 < I < S2. Sample S2 requires 15.3% of deformation faults and 31.8% of growth faults to describe its experimental pattern.

Although high amounts of defects were expected for this sample, one over two faulted layers per crystallite seems intuitively a too large value. The reduced number of layers per crystallite, which takes a value of 7 in sample S2, and the high value of D_l^{-1}, about eight times greater than the value obtained for sample S1, indicates that size effects contribute strongly to anisotropic line broadening in all the samples studied. These results, in addition to the fact that the strong anisotropic broadening was not completely modeled, as can be ascribed from the visual comparison between the calculated and experimental profile for sample S2 (see Fig. 7), led us to the consideration of another microstructural model.

Thus, the refinement of the three β-Ni(OH)$_2$ samples was also attempted by using the SH anisotropic size treatment implemented in the program FullProf. Indeed, transmission electronic microscope (TEM) images of the samples show that the crystallites are platelet-shaped, with strong shape anisotropy as they are much more wide than thick.

Final values of the main refined parameters for all the samples by using the SH size treatment are summarized in Table 2 with

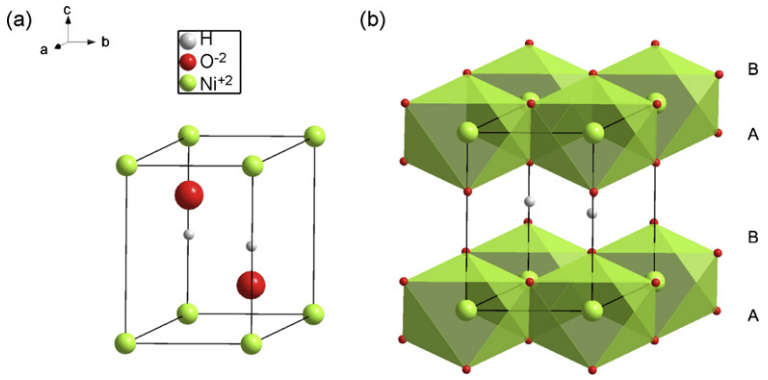

Fig. 6. Ideal structure of β-Ni(OH)$_2$: (a) unit cell atomic content and (b) unit cell viewed as edge sharing NiO_6 octahedra with an ABAB oxygen packing.

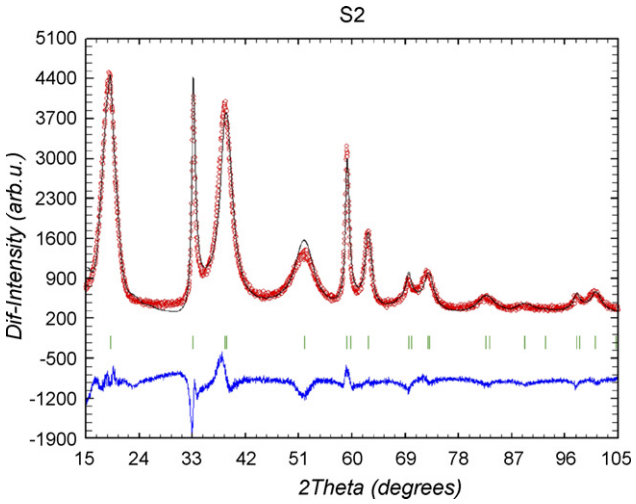

Fig. 7. Experimental X-ray powder diffraction pattern (dotted curve) compared to the FAULTS-refined profile (continuous line) and difference curve corresponding to sample S2.

the obtained crystallite sizes. A comparison between the calculated and the observed powder diffraction patterns and their difference is shown in Fig. 8a–c together with TEM micrographs of each sample and a representation of the average apparent shape of the diffraction domains in the directions indicated. All the samples were found to present a substantial degree of anisotropy in line broadening that could be modeled entirely with the SH approach. The estimated average apparent shapes suffer from some ripples due to the calculation but in all cases the obtained morphologies are of pseudo-hexagonal type, in good agreement with TEM observations. Moreover, the sizes extracted from the SH model are in very good agreement with the mean particle diameters obtained by TEM.

From these results, it is clear that in the case of nickel hydroxide, anisotropic peak broadening is mainly due to anisotropy in size and the good agreement with TEM observations confirms the validity of the SH-FullProf approach. The FAULTS treatment, although fits relatively well with the experimental results, erroneously induces the consideration that stacking faults are the main contribution to line broadening and their calculated number is hence artificially amplified. However, this does by no means imply that they are not present in the material. A care-

Table 2
Average sizes obtained by TEM and structural and micro structural Rietveld-refinement results for samples S1, S2 and I using the FullProf program: cell parameters, oxygen atomic positions, crystallite sizes in the ($h\,k\,0$) and ($0\,0\,l$) directions and agreement factor R_p

Parameter	S1	S2	I
TEM average diameter (Å)	430 (140)	117 (36)	233 (82)
a (Å)	3.13017 (5)	3.1329 (2)	3.1315 (1)
c (Å)	4.6173 (1)	4.681 (1)	4.6317 (5)
zO (Å)	0.2273 (4)	0.222 (1)	0.2314 (7)
Size ($h\,k\,0$) (Å)	476	179	346
Size ($0\,0\,l$) (Å)	140	53	109
R_p	6.68	8.25	10.0

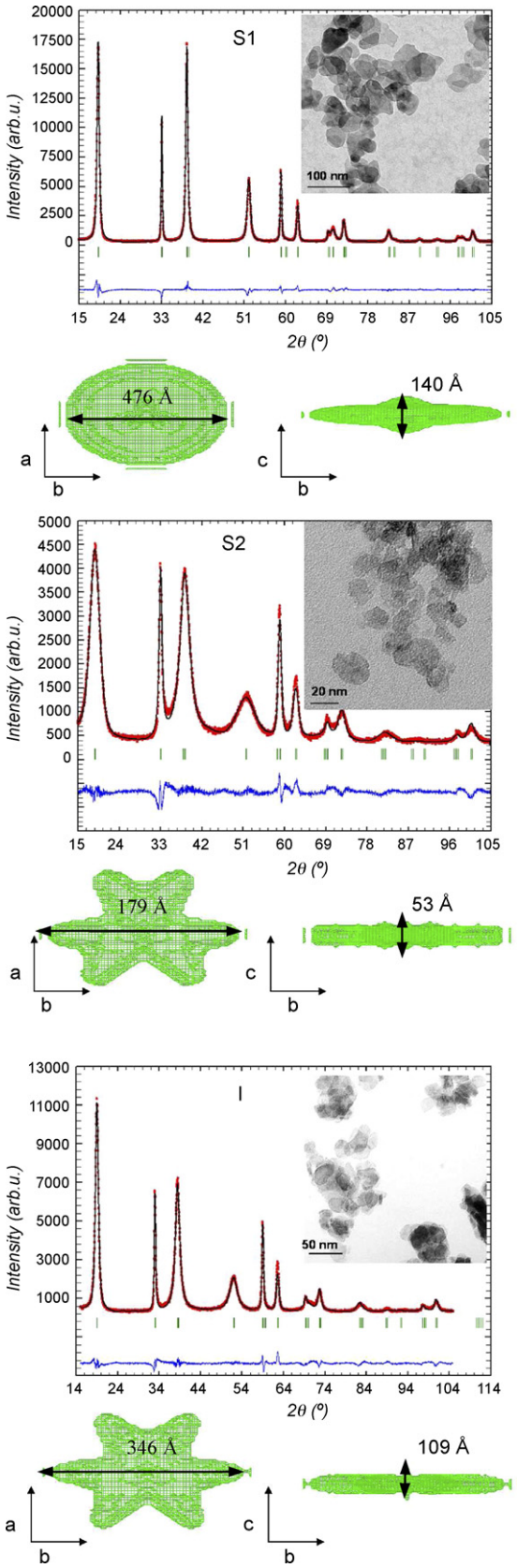

Fig. 8. Experimental X-ray powder diffraction pattern (dotted curve) compared to the Rietveld-refined profile (continuous line), difference curve, average shape and size of the crystallites in the directions indicated and TEM image of samples S1, S2 and I.

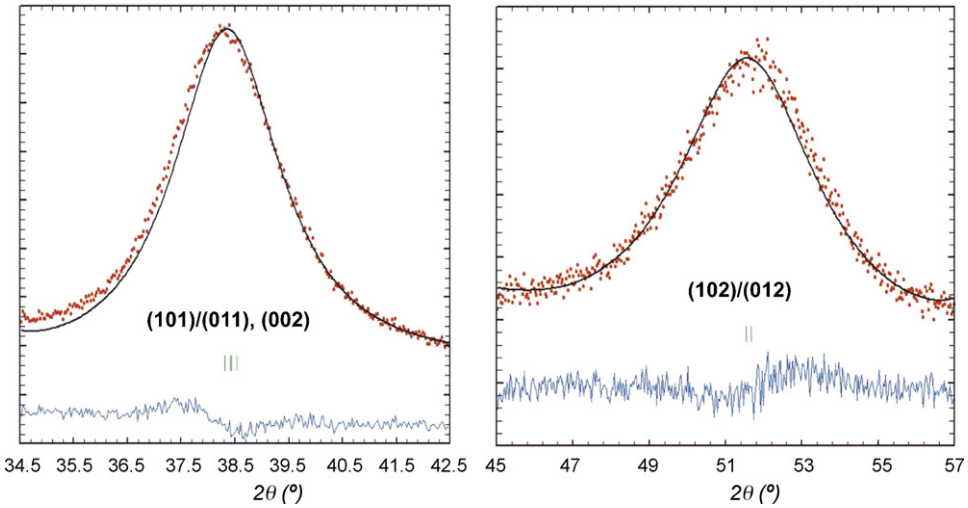

Fig. 9. Zoom of reflections (1 0 1) and (1 0 2) of sample S2 where the line shift can be appreciated when comparing the experimental profile to the Rietveld-calculated one.

ful analysis of the experimental and Rietveld-refined profile of $10l$ ($l \neq 0$) reflections reveals a line shift that was not modeled with the spherical harmonics approximation. A zoom of reflections 1 0 1 and 1 0 2 corresponding to sample S2 is displayed in Fig. 9. This line shift in reflections $10l$ ($l \neq 0$) has been reported to be also related to the existence of stacking faults [16] and has already been used to determine the probability of faulting in FCC metals [17]. Following this approach, the change in peak separation, $\delta = \Delta 2\theta_{102} - \Delta 2\theta_{101}$ has been used to give an indication of the relative degree of faulting in the material [18]. Peak displacements of the samples for reflections 1 0 1 and 1 0 2 have been determined with FullProf and the change in peak separation for each sample is detailed in Table 3.

The analysis of line shifts shows that sample S2 contains a higher amount of stacking faults than sample I and the fact that this shift was not observed in the case of sample S1 indicates that the amount of stacking faults in this sample is insignificant (if any) as all the broadening arises from instrumental and size effects. In the case of laboratory samples, the difference in the degree of faulting can be attributed to their preparation conditions. Indeed, sample S1 was prepared in the presence of a strong basic medium that favours the evolution from recently formed nuclei towards a more stable state (with a lower amount of defects) through a dissolution-recrystallization process (Ostwald ripening) [19]. In contrast, the mild conditions used in the preparation of sample S2 lead to smaller faulted crystallites. In the case of the industrial specimen the origin of the observed differences is difficult to ascertain because the details of synthesis protocol are not known.

Table 3
Change in peak separation ($\delta = \Delta 2\theta_{102} - \Delta 2\theta_{101}$) for samples S1, S2 and I

Sample	$\delta = \Delta 2\theta_{102} - \Delta 2\theta_{101}$ (°)
S1	0.00
S2	0.36
I	0.17

4. Conclusions

The microstructure of Li_2PtO_3 and β-$Ni(OH)_2$ has been studied by using two different approaches, both based in refinement of powder X-ray diffraction data.

In the Li_2PtO_3 case, Rietveld refinement of X-ray diffraction data was attempted but it was not possible to model the Warren fall. This led us to the use of the FAULTS program as it allows the refinement of different types of stacking faults and its corresponding stacking probabilities. The structure was found to consist of a random stacking of the three possible Li/Pt arrangements that maintain the honeycomb configuration. These results indicate that the FAULTS program does clearly outperform DIFFaX due to the ability to refine experimental data and is hence very suitable for the study of imperfections in this type of materials.

In the β-$Ni(OH)_2$ case, several nickel hydroxide samples with different microstructural features were refined by using the FAULTS program. The XRD patterns were well modeled, however, in the case of the least crystalline sample, too high amounts of stacking faults were obtained. The same samples were refined by using the Rietveld method with the FullProf program, using an anisotropic size broadening treatment based in linear combinations of spherical harmonics. Average size and shape of the crystallites were also obtained from the refinements that are fully consistent with TEM data. This confirms the validity of the approach and thus indicates that anisotropic peak broadening mainly comes from anisotropic size effects. The degree of stacking faults in the samples is then alternatively better estimated from the extent of shifts in reflections $10l$ where $l \neq 0$, which is not influenced by crystallite size.

The comparison of these two approaches clearly evidences that before facing X-ray diffraction data of poorly crystallized samples it is essential both to analyze all the possible contributions to line broadening and to bear in mind all the assumptions made in the approach used to ensure it is suitable for the specific case under study.

Acknowledgments

The authors would like to thank the CSIC (I3P program) the Departament d'Universitats, Recerca i Societat de la Informació de la Generalitat de Catalunya.

References

[1] M.M.J. Treacy, J.M. Newsam, M.W. Deem, Proc. R. Soc. Lond. Ser. A 433 (1991) 499–520.
[2] M. Casas-Cabanas, M.R. Palacín, J. Rodríguez-Carvajal, Z. Krist. Suppl. 23 (2006) 243–248.
[3] J. Rodriguez-Carvajal, Comission Powder Diff. Int. Union Cryst., Newsletter 26 (2001) 12–19.
[4] K. Asakura, S. Okada, A. Hajime, S. Tobishima, Y. Sakurai, J. Power Sources 81 (1999) 388–392.
[5] J. Breger, M. Jiang, N. Dupre, Y.S. Meng, Y. Shao-Horn, G. Ceder, C.P. Grey, J. Solid State Chem. 178 (2005) 2575–2585.
[6] Z.S. Wronski, G.J.C. Carpenter, P.J. Kalal, The Electrochemical Society Proceedings Series, Pennington, NJ, 1996, pp. 177–188.
[7] C. Delmas, C. Tessier, J. Mater. Chem. 7 (8) (1997) 1439–1443.
[8] C. Tessier, P.H. Haumesser, P. Bernard, C. Delmas, J. Electrochem. Soc. 146 (1999) 2059–2067.
[9] A. Audemer, Ph.D. Thesis, University of Picardie, 1997.
[10] M. Casas-Cabanas, M.R. Palacin, J. Rodriguez-Carvajal, Powder Diffract. 20 (2005) 334–344.
[11] L.B. McCusker, R.B. Von Dreele, D.E. Cox, D. Louër, P. Scardi, J. Appl. Cryst. 32 (1999) 36–50.
[12] P. Thompson, D.E. Cox, J.B. Hastings, J. Appl. Cryst. 20 (1987) 79–83.
[13] J. González-Platas, J. Rodriguez-Carvajal, Graphic Fourier Program GFOURIER Version 04.02, Univ. La Laguna, Tenerife, Spain, 2002.
[14] Y. Laligant, P. Lacorre, J. Rodriguez-Carvajal, Mater. Sci. Forum 378 (2001) 632–637.
[15] C. Greaves, M.A. Thomas, Acta Crystallogr. B 42 (1986) 51–55.
[16] B.E. Warren, X-Ray Diffraction, Dover Publications, New York, 1990, p. 275.
[17] B.E. Warren, E.P. Wakerois, J. Appl. Phys. 24 (1953) 951–952.
[18] M. Casas-Cabanas, J. Canales-Vázquez, J. Rodriguez-Carvajal, M.R. Palacin, J. Chem. Mater. 16 (28) (2006) 2925–2939.
[19] W. Ostwald, Z. Phys. Chem. 34 (1900) 495–503.